IEEE Access
Multidisciplinary | Rapid Review | Open Access Journal

Received February 8, 2020, accepted February 24, 2020, date of publication February 28, 2020, date of current version March 12, 2020.

*Digital Object Identifier 10.1109/ACCESS.2020.2977270*

# Dynamic Phasor Modeling of Various Multipulse Rectifiers and a VSI Fed by 18-Pulse Asymmetrical Autotransformer Rectifier Unit for Fast Transient Analysis

**DONGSHENG YUAN[1,2], (Student Member, IEEE), SHUHONG WANG[1,3], (Senior Member, IEEE), AND YILU LIU[2,4], (Fellow, IEEE)**

[1]Department of Electrical Engineering, Xi'an Jiaotong University, Xi'an 710079, China
[2]Department of Electrical Engineering and Computer Science, The University of Tennessee at Knoxville, Knoxville, TN 37996, USA
[3]State Key Laboratory of Electrical Insulation and Power Equipment, Xi'an 710079, China
[4]Oak Ridge National Laboratory, Oak Ridge, TN 37831, USA

Corresponding author: Shuhong Wang (shwang@mail.xjtu.edu.cn)

**ABSTRACT** To study the fast modelling of dynamic characteristics caused by power electronic switching, the dynamic phasor (DP) theory based on the time-varying Fourier decomposition and frequency shifting is firstly applied to the modelling of various multipulse rectifiers. The DP model for symmetrical 12-pulse phase-shifting reactor rectifier unit (PSR-RU) is derived with model order reduction, relations between ac and dc terminals, and Taylor series expansion. The DP model of asymmetrical 18-pulse autotransformer rectifier unit (AT-RU) is proposed based on the switching functions expressed in the DP domain. Meanwhile, the DP model of voltage source inverter (VSI) fed by asymmetrical 18-pulse AT-RU is built with the harmonic state-space (HSS) equations. Under both balanced and unbalanced conditions, the good calculation accuracy and rapid simulation speed of the developed DP models are validated by the detailed time-domain (TD) simulation.

**INDEX TERMS** Dynamic phasor, transient analysis, quick simulation, multipulse rectifier, voltage source inverter.

## NOMENCLATURE

| | |
|---|---|
| EPS | Electric power system |
| TD | Time domain |
| DP | Dynamic phasor |
| DPs | Dynamic phasors |
| DB | Diode bridge |
| QSS | Quasi-steady-state |
| HSS | Harmonic state-space |
| AT-RU | Autotransformer rectifier unit |
| PSR | Phase-shifting reactor |
| VSI | Voltage source inverter |
| SPWM | Sinusoidal pulse width modulation |
| THD | Total harmonic distortion |
| RMS | Root mean square value |
| $x(\tau)$ | Time domain quasi-periodic signal |
| $x(t)$ | Time domain periodic signal |
| $< x >_k$ | $k$th dynamic phasor |
| $t, \tau$ | Time |
| $p$ | Coefficient of Taylor series |
| $s$ | Switching function |
| $J_p$ | Bessel Function |
| $N$ | Winding turns |
| $\omega_s$ | Angular frequency of fundamental wave |
| $\omega_r$ | Angular frequency of reference signal |
| $\rho$ | Pearson's correlation coefficient |
| $i_A, i_B, i_C$ | Power source side ac current |
| $u_{V1}, u_{W1}, u_{U1}$ | Voltages fed to the diode bridge |

The associate editor coordinating the review of this manuscript and approving it for publication was B. Chitti Babu.

| | |
|---|---|
| $\boldsymbol{u}_{\text{lead}}$ | Voltage vector of Voltages fed to the phase-lead diode bridge in 12-pulse PSR |
| $u_{\text{dc}}$ | Rectifier dc-side voltage |
| $i_{\text{dc}}$ | Rectifier dc-side current |
| $i_{\text{U}}$, $i_{\text{V}}$, $i_{\text{W}}$ | Inverter ac-side current |
| $R$ | Rectifier dc-side resistor load |
| $L$ | Rectifier dc-side inductor load |
| $C$ | Rectifier dc-side capacitor load |

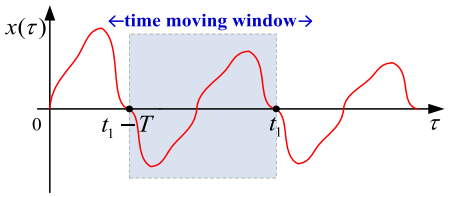


**FIGURE 1.** The waveform of the time-domain quasi-periodic signal.

## I. INTRODUCTION

The modern electric power system (EPS) generally comprises many different power converters and contains magnetic devices and power electronic components. The dynamic processes of EPS are with different time constants, such as electromagnetic motion and electronic motion. The structural complexity and multi-time scale transients make the dynamic characteristic analysis of power system to be challenging [1]–[4]. To evaluate the system efficiency, power quality, and dynamic performance efficiently, a quick and precise simulation method with time-varying properties is required [5], [6].

The multipulse rectifier unit consisting of magnetic parts and power electronic components is an essential ac/dc power conversion device in the EPS [7], [8]. A large number of multipulse rectifier units have been used in the EPS because of their simple configuration, high reliability, and low electromagnetic interference [9]–[11]. Thus, this paper aims to simulate the dynamic characteristics of multipulse rectifier units with an efficient method.

The detailed time-domain (TD) modelling and the state-space averaging modelling are two general simulation methods. The TD modelling is accurate but too time-consuming for an extensive power conversion system. The state-space averaging modelling with the quasi-steady-state (QSS) assumption is fast, but it cannot reveal the harmonic dynamics of the power conversion system. Meanwhile, the fast simulation methods of multipulse rectifier units are studied. Reference [12] proposes a functional model for the symmetrical 18-pulse autotransformer rectifier unit (AT-RU), where the 3-9-dc system is simplified to a 3-3-dc system. Reference [13] achieves the fast simulation of 12-pulse AT-RU by representing the three-phase diode bridge with a dc transformer. These two models are based on the fundamental switching function and Park's transformation, the evaluation for ac current harmonics and dc voltage ripple is unavailable, and the second harmonics dramatically decreases the simulation speed under the unbalanced condition.

The generalized averaging technique, which is also called as the dynamic phasor (DP) method, is firstly presented in [14]. This method can be applied in periodically or nearly periodically driven systems. Due to higher calculation accuracy than the QSS model and faster simulation speed than the detailed TD model, the DP method has been used in modelling of three-phase thyristor controlled reactor [15], high voltage direct current systems [16], and multi-generator power systems [17]. However, the DP simulation of multipulse rectifier units is not reported before.

Different forms to exhibit the DP model have been used in the relevant references. In [18], the DP model of a three-phase diode bridge is stated by transforming the time-domain mathematical expressions between ac and dc terminal into the DP domain. The DP models elaborated in [19]–[23] are expressed with the harmonic state-space (HSS) equations. Both approaches are adopted in this paper to make the DP modelling of multipulse rectifier units convenient.

Based on the DP theory, this paper aims to provide a solution to model the multipulse rectifiers, and extended power system with multipulse rectifiers efficiently and accurately. Here, only the effects caused by nonlinear power electronic switching are considered, the effects of nonlinear magnetic properties will be discussed in a separate work. The paper is organized as follows. Section II revises the DP theory. Section III introduces the DP model of three-phase diode bridges into the modelling of symmetrical 12-pulse phase-shifting reactor rectifier unit (PSR-RU), its applicability in the modelling of symmetrical multipulse rectifier units as a library element is also validated. Section IV proposes the DP model of asymmetrical 18-pulse AT-RU. Section V puts forward the DP model of voltage source inverter (VSI) fed by 18-pulse AT-RU, verifying that the DP model of multipulse RU is of good applicability and transplantability within the extended EPS models. Section VI shows the computation efficiency of the developed DP models, and Section VII concludes the paper.

## II. DYNAMIC PHASOR THEORY

Under the QSS assumption, the average of state-variable $x(t)$ throughout $T$ is defined as

$$\langle x \rangle (t) = 1/T \cdot \int_{t-T}^{t} x(\tau) d\tau \tag{1}$$

where $T$ is the period of the fundamental component.

To a time-domain quasi-periodic signal $x(\tau)$ without QSS assumption, as shown in Fig. 1, it can be regarded as a periodic signal at the time moving window $\tau \in (t_1 - T, t_1]$.

Hence, $x(\tau)$ can be represented as

$$x(\tau) = \sum\nolimits_{k=-\infty}^{\infty} X_k(t) e^{jk\omega_s \tau}, \quad \tau \in (t - T, t] \tag{2}$$

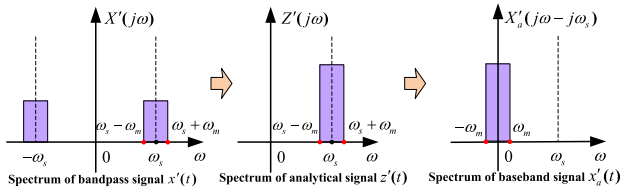


**FIGURE 2.** The baseband representation of quasi-steady state signal.

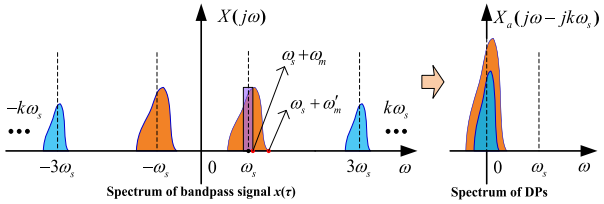


**FIGURE 3.** The baseband representation of the quasi-periodic signal.

where the $k$th Fourier coefficients $X_k(t)$ are the $k$th Dynamic phasors (DPs) [14]

$$\langle x\rangle_k = X_k(t) = 1/T\int_{t-T}^{t} x(\tau)e^{-jk\omega_s\tau}d\tau \tag{3}$$

The DPs of $x(\tau)$ are with time-varying properties. Formula (3) equals to (1) when $k$ is 0, that means one could retain only the 0th DP in this generalized averaging method to recover the traditional state-space averaging model.

To the signal $x'(t) = a(t)\cos[\omega_s t + \theta(t)]$ under QSS assumption, the variation of amplitude $a(t)$ and phase angle $\theta(t)$ are minimal when compared with $\omega_s$. Here, $\omega_s$ corresponds to the fundamental component of the system. As shown in Fig. 2, $x'(t)$ can be represented with its analytical signal $z'(t) = a(t)e^{j\theta(t)}e^{j\omega st}$ by discarding the negative frequency component. Furtherly, $z'(t)$ is frequency shifted to the baseband signal $x'_a(t) = a(t)e^{j\theta(t)}$, and $x'_a(t)$ is the fundamental phasor of $x'(t)$. The baseband representation makes it possible to use a large simulation time step, and this is the reason using phasor representation under the steady-state condition.

Unlike $a(t)$ and $\theta(t)$ of $x'(t)$ under the QSS assumption, $X_k(t)$ in (3) are time-varying and have wider bandwidth. As shown in Fig. 3, all the frequency components of time-varying signal $x(\tau)$ can be transformed into the baseband signals $X_k(t)$. Hence the DP representation method meets simulation requirements of the power electronics dominated power system for the high calculation accuracy and fast simulation speed.

The crucial properties of DPs are given below [16], [17].

First, the relationship between derivatives of variable $x(\tau)$ and derivatives of $k$th DP $X_k(t)$ is

$$\langle \mathrm{d}x(\tau)/\mathrm{d}t\rangle_k = \mathrm{d}X_k(t)/\mathrm{d}t + jk\omega_s X_k(t) \tag{4}$$

Second, the product of two time-domain variables equals the discrete-time convolution of corresponding DPs

$$\langle xy\rangle_k = \sum\nolimits_i \langle x\rangle_{k-i}\langle y\rangle_i \tag{5}$$

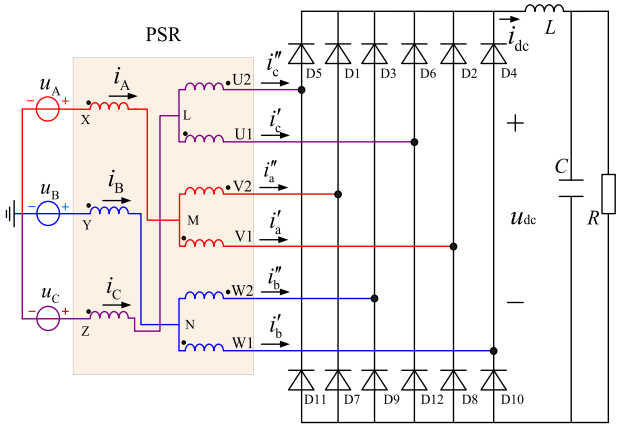


**FIGURE 4.** The circuit topology of 12-pulse PSR-RU.

Third, the relationship between $X_k(t)$ and its complex conjugate $X_k^*(t)$ is

$$X_{-k}(t) = X_k^*(t) \tag{6}$$

The time-domain signal can be restored from DPs as

$$x(\tau) = X_0(t) + 2\cdot \mathrm{Re}\left\{\sum\nolimits_{k=1}^{\infty} X_k(t)e^{jk\omega_s\tau}\right\} \tag{7}$$

## III. DP MODELLING FOR SYMMETRICAL 12-PULSE PSR-RU

The 12-pulse PSR-RU discussed in [11] is taken as an example to evaluate the applicability of diode bridges DP model in the modelling of multipulse rectifier unit [18].

Fig. 4 depicts the circuit topology of 12-pulse PSR-RU. PSR-RU with small volume capacity works in series. The input windings $W_{XM}$, $W_{YN}$, and $W_{ZL}$ connect with the power source, the output windings $W_{LU2}$, $W_{LU1}$, $W_{MV2}$, $W_{MV1}$, $W_{NW2}$, and $W_{NW1}$ connect with diode bridges. The winding turn satisfy $N_{XM} = N_{YN} = N_{ZL}$, $N_{V1M} = N_{W1N} = N_{U1L}$, $N_{V2M} = N_{W2N} = N_{U2L}$, and $N_{V1M} = N_{YN} + N_{V2M}$. With this kind of connection mode, the phase of $i_a$' and $i_a$'' are ahead and lag of the phase of $i_A$ with the same angle $\theta$. Based on the principle of minimum Total Harmonic Distortion (THD), the phase-shifting angle $\theta$ is $\theta = \pi/12$. The fundamental current of $i_A$ basically remain unchanged, while the $n$th harmonic current would be reduced effectively.

The current and voltage phasor diagram of phase A is plotted in Fig. 5, only the fundamental phasors are given here. $\theta = \pi/12$ is the phase-shifting angle; $\varphi$ is the impedance angle. The effect of 5th and 7th harmonic currents of $i'_a$ and $i''_a$ can be significantly reduced because of their phase differences is about $\pi$. $u_{v1}$ and $u_{v2}$ are with the same amplitude and $\pi/6$ phase difference. Hence, it is reasonable to transform the 12-pulse PSR-RU into two symmetrical three-phase diode bridges.

According to the voltage phasor diagram shown in Fig. 5, the relationship between voltages fed to diode bridges and

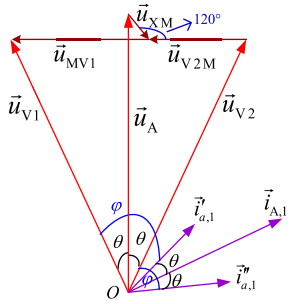


**FIGURE 5.** The fundamental current and voltage phasor diagram of the PSR.

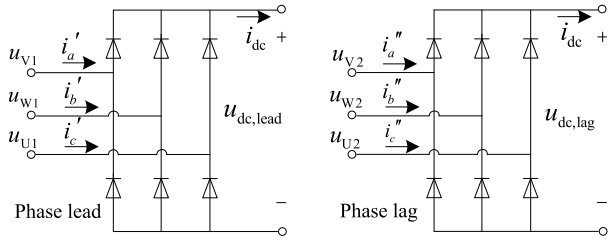


**FIGURE 6.** The two separated diode bridges in 12-pulse PSR-RU.

voltages in the power source side can be obtained as

$$\begin{cases} u_{V1} = 1/2\sqrt{3}(k_3+k_2)(u_C-u_B)+(1-\sqrt{3}/2k_1)u_A \\ u_{W1} = 1/2\sqrt{3}(k_3+k_2)(u_A-u_C)+(1-\sqrt{3}/2k_1)u_B \\ u_{U1} = 1/2\sqrt{3}(k_3+k_2)(u_B-u_A)+(1-\sqrt{3}/2k_1)u_C \end{cases}$$
$$\begin{cases} u_{V2} = -1/2\sqrt{3}(k_3+k_2)(u_C-u_B)+(1-\sqrt{3}/2k_1)u_A \\ u_{W2} = -1/2\sqrt{3}(k_3+k_2)(u_A-u_C)+(1-\sqrt{3}/2k_1)u_B \\ u_{U2} = -1/2\sqrt{3}(k_3+k_2)(u_B-u_A)+(1-\sqrt{3}/2k_1)u_C \end{cases} \quad (8)$$

where,

$$\begin{cases} k_1 = 2\sqrt{3}(1-\cos^2\theta)/3 \\ k_2 = (\cos\theta\sin\theta+\sqrt{3(1-\cos^2\theta)/3}) \\ k_3 = (\cos\theta\sin\theta-\sqrt{3(1-\cos^2\theta)/3}) \end{cases} \quad (9)$$

Meanwhile, the relationship between input and output terminal currents are

$$\begin{cases} i_A = i'_a + i''_a \\ i_B = i'_b + i''_b \\ i_C = i'_c + i''_c \end{cases} \quad (10)$$

The diode bridges in the 12-pulse PSR-RU can be separated into two three-phase diode bridges, as shown in Fig. 6. They are named as phase lead diode bridges and phase lag diode bridges, respectively.

Here, only DP modelling of phase lead diode bridges is analyzed due to the similarity.

The input voltages can be written as

$$u_i(t) = U_i\cos(\omega t+\varphi_i), \quad i = \text{V1, W1, U1} \quad (11)$$

With Euler formulate and DP definition, (12) is valid

$$\begin{aligned} u_i(t) &= 1/2\cdot V_i e^{j\varphi_i}e^{j\omega t} + 1/2\cdot V_i e^{-j\varphi_i}e^{-j\omega t} \\ &= \langle u_i\rangle_1 e^{j\omega t} + \langle u_i\rangle_{-1} e^{-j\omega t} \quad i = \text{V1, W1, U1} \end{aligned} \quad (12)$$

As revealed in (8), DPs of $u_i(t)$, $i$ = V1, W1, U1, can be obtained from the power source voltages under both balanced and unbalanced conditions. Assuming $\boldsymbol{u}_{\text{lead}}$ is the voltage vector representation of $u_i(t)$, the relationship between $\boldsymbol{u}_{\text{lead}}$ and three input voltages in DP domain is as below

$$\begin{aligned} \boldsymbol{u}_{\text{lead}}e^{-j\omega t} &= \boldsymbol{u}_{\text{d, lead}} + j\boldsymbol{u}_{\text{q, lead}} \\ &= \frac{2}{3}[\langle u_{V1}\rangle_1 + \langle u_{W1}\rangle_1 e^{j\cdot 2\pi/3} + \langle u_{U1}\rangle_1 e^{-j\cdot 2\pi/3}] \\ &\quad + \frac{2}{3}e^{-j2\omega t}[\langle u_{V1}\rangle_1^* + \langle u_{W1}\rangle_1^* e^{j\cdot 2\pi/3} \\ &\quad + \langle u_{U1}\rangle_1^* e^{-j\cdot 2\pi/3}] \end{aligned} \quad (13)$$

Therefore, the dq components of $\boldsymbol{u}_{\text{lead}}$ in DP domain can be derived as

$$\begin{cases} \boldsymbol{u}_{\text{d, lead}} = U_{\text{d, lead,0}}\cdot e^{j(0\cdot\omega t)} \\ \quad + \dfrac{U_{\text{d, lead,2}} - jU_{\text{q, lead,2}}}{2}\cdot e^{j(2\cdot\omega t)} \\ \quad + \dfrac{U_{\text{d, lead,2}} + jU_{\text{q, lead,2}}}{2}\cdot e^{j(-2\cdot\omega t)} \\ \quad = \langle u_{\text{d, lead}}\rangle_0\cdot e^{j(0\cdot\omega t)} + \langle \boldsymbol{u}_{\text{d, lead}}\rangle_2\cdot e^{j(2\cdot\omega t)} \\ \quad + \langle \boldsymbol{u}_{\text{d, lead}}\rangle_{-2}\cdot e^{j(-2\cdot\omega t)} \\ \boldsymbol{u}_{\text{q, lead}} = U_{\text{q, lead,0}}\cdot e^{j(0\cdot\omega t)} \\ \quad + \dfrac{U_{\text{q, lead,2}} + jU_{\text{d, lead,2}}}{2}\cdot e^{j(2\cdot\omega t)} \\ \quad + \dfrac{U_{\text{q, lead,2}} - jU_{\text{d, lead,2}}}{2}\cdot e^{j(-2\cdot\omega t)} \\ \quad = \langle u_{\text{q, lead}}\rangle_0\cdot e^{j(0\cdot\omega t)} + \langle \boldsymbol{u}_{\text{q, lead}}\rangle_2\cdot e^{j(2\cdot\omega t)} \\ \quad + \langle \boldsymbol{u}_{\text{q, lead}}\rangle_{-2}\cdot e^{j(-2\cdot\omega t)} \end{cases} \quad (14)$$

where,

$$\begin{aligned} &U_{\text{d, lead,0}} \\ &\quad = 2/3\cdot\text{Re}\left[\langle u_{V1}\rangle_1 + \langle u_{W1}\rangle_1 e^{j\cdot 2\pi/3} + \langle u_{U1}\rangle_1 e^{-j\cdot 2\pi/3}\right] \\ &U_{\text{q, lead,0}} \\ &\quad = 2/3\cdot\text{Im}\left[\langle u_{V1}\rangle_1 + \langle u_{W1}\rangle_1 e^{j\cdot 2\pi/3} + \langle u_{U1}\rangle_1 e^{-j\cdot 2\pi/3}\right] \\ &U_{\text{d, lead,2}} \\ &\quad = 2/3\cdot\text{Re}\left[\langle u_{V1}\rangle_1^* + \langle u_{W1}\rangle_1^* e^{j\cdot 2\pi/3} + \langle u_{U1}\rangle_1^* e^{-j\cdot 2\pi/3}\right] \\ &U_{\text{q, lead,2}} \\ &\quad = 2/3\cdot\text{Im}\left[\langle u_{V1}\rangle_1^* + \langle u_{W1}\rangle_1^* e^{j\cdot 2\pi/3} + \langle u_{U1}\rangle_1^* e^{-j\cdot 2\pi/3}\right] \end{aligned} \quad (15)$$

Without considering the dc voltage drop caused by commutation effect, the time-domain dc voltage $u_{\text{dc,lead}}$ can be represented with dq components of $\boldsymbol{u}_{\text{lead}}$

$$u_{\text{dc, lead}} = \frac{3\sqrt{3}}{\pi}\sqrt{\boldsymbol{u}_{\text{d, lead}}^2 + \boldsymbol{u}_{\text{q, lead}}^2} \quad (16)$$

Hence, $u_{\text{dc,lead}}$ can be restored with DPs by expanding (16) into Taylor series concerning $\boldsymbol{u}_{\text{d,lead}}$ and $\boldsymbol{u}_{\text{q,lead}}$ [18].

$$u_{\text{dc, lead}} = \langle u_{\text{dc, lead}}\rangle_0 + 2\cdot\langle u_{\text{dc, lead}}\rangle_2 e^{j2\omega t} + 2\cdot\langle u_{\text{dc, lead}}\rangle_4 e^{j4\omega t} \quad (17)$$

where,

$$\begin{aligned}\langle u_{\mathrm{dc,\,lead}}\rangle_0 &= p_0 + p_3\langle u_{\mathrm{d,\,lead}}\rangle_2\langle u_{\mathrm{d,\,lead}}\rangle_{-2} \\ &\quad + p_4\langle u_{\mathrm{q,\,lead}}\rangle_2\langle u_{\mathrm{q,\,lead}}\rangle_{-2} \\ &\quad + p_5/2\cdot\left(\langle u_{\mathrm{d,\,lead}}\rangle_2\langle u_{\mathrm{q,\,lead}}\rangle_{-2}\right. \\ &\quad \left. + \langle u_{\mathrm{d,\,lead}}\rangle_{-2}\langle u_{\mathrm{q,\,lead}}\rangle_2\right) \\ \langle u_{\mathrm{dc,\,lead}}\rangle_2 &= p_1\langle u_{\mathrm{d},lead}\rangle_2 + p_2\langle u_{\mathrm{q,\,lead}}\rangle_2 \\ \langle u_{\mathrm{dc,\,lead}}\rangle_4 &= p_3/2!\cdot\left(\langle u_{\mathrm{d,\,lead}}\rangle_2\right)^2 + p_4/2!\cdot\left(\langle u_{\mathrm{q,\,lead}}\rangle_2\right)^2 \\ &\quad + p_5/2!\cdot\left(\langle u_{\mathrm{d,\,lead}}\rangle_2\langle u_{\mathrm{q,\,lead}}\rangle_2\right) \end{aligned} \tag{18}$$

$p_m(m = 0, 1, \ldots, 5)$ are the coefficients of Taylor series at point $(U_{\mathrm{d,lead},0}, U_{\mathrm{q,lead},0})$.

$$\begin{cases} p_0 = f_1(U_{\mathrm{d,\,lead},0}, U_{\mathrm{q,\,lead},0}) \\ \quad = 3\sqrt{3}/\pi\cdot\sqrt{U^2_{\mathrm{d,\,lead},0} + U^2_{\mathrm{q,\,lead},0}} \\ p_1 = \dfrac{\partial f_1(U_{\mathrm{d,\,lead},0}, U_{\mathrm{q,\,lead},0})}{\partial U_{\mathrm{d,\,lead},0}} \\ \quad = \dfrac{3\sqrt{3}}{\pi}\cdot\dfrac{U_{\mathrm{d,\,lead},0}}{\sqrt{U^2_{\mathrm{d,\,lead},0} + U^2_{\mathrm{q,\,lead},0}}} \\ p_2 = \dfrac{\partial f_1(U_{\mathrm{d,\,lead},0}, U_{\mathrm{q,\,lead},0})}{\partial U_{\mathrm{q,\,lead},0}} \\ \quad = \dfrac{3\sqrt{3}}{\pi}\dfrac{U_{\mathrm{q,\,lead},0}}{\sqrt{U^2_{\mathrm{d,\,lead},0} + U^2_{\mathrm{q,\,lead},0}}} \\ p_3 = \dfrac{\partial^2 f_1(U_{\mathrm{d,\,lead},0}, U_{\mathrm{q,\,lead},0})}{\partial U^2_{\mathrm{d,\,lead},0}} \\ \quad = \dfrac{3\sqrt{3}}{\pi}\dfrac{(U_{\mathrm{q,\,lead},0})^2}{(U^2_{\mathrm{d,\,lead},0} + U^2_{\mathrm{q,\,lead},0})^{3/2}} \\ p_4 = \dfrac{\partial^2 f_1(U_{\mathrm{d,\,lead},0}, U_{\mathrm{q,\,lead},0})}{\partial U^2_{\mathrm{q,\,lead},0}} \\ \quad = \dfrac{3\sqrt{3}}{\pi}\dfrac{(U_{\mathrm{d,\,lead},0})^2}{(U^2_{\mathrm{d,\,lead},0} + U^2_{\mathrm{q,\,lead},0})^{3/2}} \\ p_5 = 2\dfrac{\partial^2 f_1(U_{\mathrm{d,\,lead},0}, U_{\mathrm{q,\,lead},0})}{\partial U_{\mathrm{d,\,lead},0}\partial U_{\mathrm{q,\,lead},0}} \\ \quad = -2\dfrac{3\sqrt{3}}{\pi}\dfrac{U_{\mathrm{d,\,lead},0}U_{\mathrm{q,\,lead},0}}{(U^2_{\mathrm{d,\,lead},0} + U^2_{\mathrm{q,\,lead},0})^{3/2}} \end{cases} \tag{19}$$

Formula (16) is derived without considering the affection of harmonic components. The 6th harmonic of dc voltage caused by 5th and 7th switching harmonics is given as

$$\langle u_{\mathrm{dc,\,lead}}\rangle_6 = r\cdot\left(1/2\cdot u_{\mathrm{dc,\,lead},6}e^{j\varphi_{\mathrm{dc,\,lead},6}}\right) \tag{20}$$

where,

$$\begin{cases} u_{\mathrm{dc,\,lead},6} = -\dfrac{3\sqrt{3}}{5\pi}\sqrt{V^2_{\mathrm{d,\,lead},0} + V^2_{\mathrm{q,\,lead},0}} \\ \quad + \dfrac{3\sqrt{3}}{7\pi}\sqrt{V^2_{\mathrm{d,\,lead},0} + V^2_{\mathrm{q,\,lead},0}} \\ \varphi_{\mathrm{dc,\,lead},6} = 6\tan^{-1}(V_{\mathrm{q,\,lead},0}/V_{\mathrm{d,\,lead},0}) \end{cases} \tag{21}$$

$r = 1/2$ is used to compensating the voltage ripple difference between 12-pulse rectifier and simplified 6-pulse rectifier. Finally, $u_{\mathrm{dc,lead}}$ can be recovered from its corresponding DPs.

$$u_{\mathrm{dc,\,lead}}(t) = \langle u_{\mathrm{dc,\,lead}}\rangle_0 + 2\cdot\mathrm{Re}\left\{\sum\nolimits_{k=2,4,6}\langle u_{\mathrm{dc,\,lead}}\rangle_k\cdot e^{jk\omega t}\right\} \tag{22}$$

Assuming $< i_{\mathrm{dc}} >_0 = i_{\mathrm{dc}}(t)$, that means the 0th DP contains all information of current $i_{\mathrm{dc}}(t)$ [18]. For the phase lead diode bridges, the vector of the input current is $\boldsymbol{i}_{\mathrm{m,lead}}$, and it has $< i_{\mathrm{m,lead}} >_0 = \boldsymbol{i}_{\mathrm{m,lead}}$. The relationship between $\boldsymbol{i}_{\mathrm{m,lead}}$ and $i_{\mathrm{dc}}$ is as follows:

$$\langle i_{\mathrm{m,\,lead}}\rangle_0 = 1/2\cdot\left(2\sqrt{3}/\pi\cdot\langle i_{\mathrm{dc}}\rangle_0\right) = \sqrt{3}/\pi\cdot i_{\mathrm{dc}} \tag{23}$$

The dq components of $\boldsymbol{i}_{\mathrm{m,lead}}$ in DP domain are as below

$$\begin{cases} \langle i_{\mathrm{d,\,lead}}\rangle_n = \sum\nolimits_{n=0,\pm2,\pm4}\langle i_{\mathrm{m,\,lead}}\rangle_0\langle\cos\varphi_{\mathrm{lead}}\rangle_n \\ \langle i_{\mathrm{q,\,lead}}\rangle_n = \sum\nolimits_{n=0,\pm2,\pm4}\langle i_{\mathrm{m,\,lead}}\rangle_0\langle\sin\varphi_{\mathrm{lead}}\rangle_n \end{cases} \tag{24}$$

Besides,

$$\begin{aligned}\cos\varphi_{\mathrm{lead}} &= f(u_{\mathrm{d,\,lead}}, u_{\mathrm{q,\,lead}}) \\ &= u_{\mathrm{d,\,lead}}/\sqrt{(u_{\mathrm{d,\,lead}})^2 + (u_{\mathrm{q,\,lead}})^2} \\ \sin\varphi_{\mathrm{lead}} &= f(u_{\mathrm{d,\,lead}}, u_{\mathrm{q,\,lead}}) \\ &= u_{\mathrm{q,\,lead}}/\sqrt{(u_{\mathrm{d,\,lead}})^2 + (u_{\mathrm{q,\,lead}})^2}\end{aligned} \tag{25}$$

Similar to (16), DPs of cos $\varphi_{\mathrm{lead}}$*and* sin $\varphi_{\mathrm{lead}}$ can be obtained by using the Taylor expansion method.

Furthermore, the time-domain expressions of $i_{\mathrm{d,lead}}$ and $i_{\mathrm{q,lead}}$ can be recovered from their DPs representation as

$$\begin{cases} i_{\mathrm{d,\,lead}} = \langle i_{\mathrm{d,\,lead}}\rangle_0 + 2\cdot\mathrm{Re}[\sum\nolimits_{n=2,4}\langle i_{\mathrm{d,\,lead}}\rangle_n e^{jn\omega t}] \\ i_{\mathrm{q,\,lead}} = \langle i_{\mathrm{q,\,lead}}\rangle_0 + 2\cdot\mathrm{Re}[\sum\nolimits_{n=2,4}\langle i_{\mathrm{q,\,lead}}\rangle_n e^{jn\omega t}] \end{cases} \tag{26}$$

Based on (9), (23) and dq0/abc transformation, the time-domain value of $i_{\mathrm{A}}(t)$, $i_{\mathrm{B}}(t)$, and $i_{\mathrm{C}}(t)$ can be derived.

Assuming the RMS value of the voltage source in Fig. 4 is 220V, $u_{\mathrm{A}}$ becomes zero at time $t = 1.0$s; the frequency is 50Hz; the dc side load consists of $L = 1200\mu$H, $C = 500\mu$F, $R = 25\Omega$. The parameters of core and winding for PSR are the same as [11]. The detailed TD model built with MATLAB/Simulink is used as a benchmark, where the PSR is represented with nine dimensions inductance matrix. The dc side voltage and ac side currents gained from the two models are shown in Fig. 7 and Fig. 8.

For the symmetrical 18-pulse AT-RU, three sets of voltages are produced by symmetrical AT and fed to three three-phase diode bridges. These voltages are with the same magnitude and $2\pi/9$ phase shift. Each diode in the three-phase diode bridges has the same conducting period. The modelling of diode bridges in symmetrical 18-pulse AT-RU can be simplified to one three-phase diode bridges [12]. However, three sets of voltages produced by asymmetrical AT are with different magnitudes, and diode bridges in various three-phase diode bridges have different conducting period. Thus, the DP model of three-phase diode bridges cannot be directly used in the modelling of asymmetrical 18-pulse AT-RU.

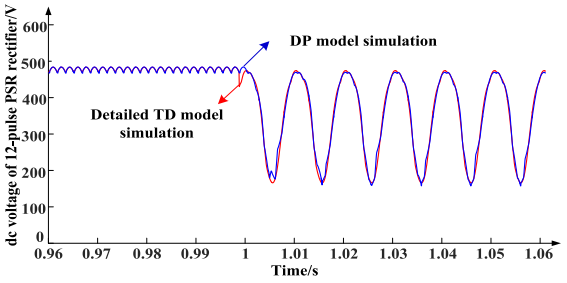


**FIGURE 7.** The dc side voltage of 12-pulse PSR-RU.

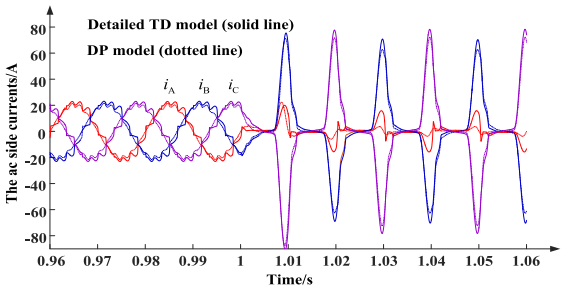


**FIGURE 8.** The ac side currents of 12-pulse PSR-RU.

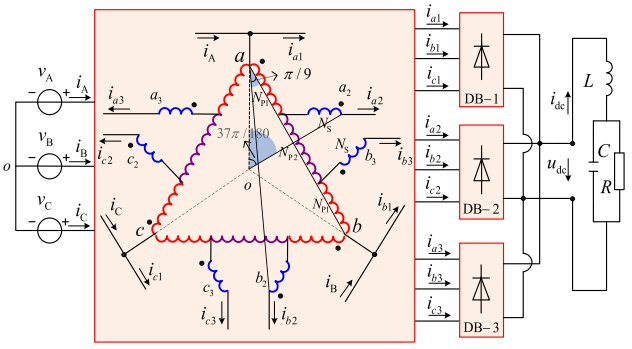


**FIGURE 9.** The circuit topology of asymmetrical 18-pulse AT-RU.

## IV. DYNAMIC MODELLING FOR THE ASYMMETRICAL 18-PULSEAT-RU

The asymmetrical 18-pulse AT-RU is shown in Fig. 9. DB-1, DB-2, and DB-3 are three three-phase diode bridges. DB-1 is directly powered by the power source ($v_a$, $v_b$, $v_c$). The primary windings of AT are triangle-connected to the power source, two taps derived from each primary winding connect the secondary windings of other two cores. Two additional three-phase voltages ($v_{a2}$, $v_{b2}$, $v_{c2}$) and ($v_{a3}$, $v_{b3}$, $v_{c3}$) are formed by vector superposition. DB-2, and DB-3 are driven by these two auxiliary three-phase voltages. The phase-shifting angle between $v_a$ and $v_{a2}$, $v_a$ and $v_{a3}$ are $37\pi/180$, the phase-shifting angle between adjacent 18 sets of line voltage is $\pi/9$. Fig. 10 illustrates the voltages fed to diode bridges of asymmetrical 18-pulse AT-RU.

In Fig. 9, $v_a$, $v_b$, and $v_c$ are equal to the power source voltages $v_A$, $v_B$, and $v_C$. The relationship between the voltages fed to diode bridges and the power source voltages are given

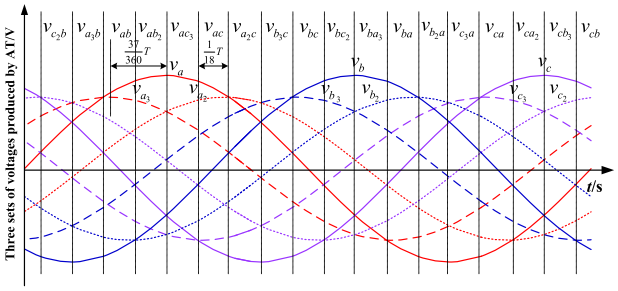


**FIGURE 10.** The waveforms of voltages fed to diode bridges.

as

$$\begin{cases} v_{a_2} = f_1(v_a, v_b, v_c) = (1-q_1)v_a + (q_1+q_2)v_b - q_2 v_c \\ v_{b_2} = f_2(v_a, v_b, v_c) = -q_2 v_a + (1-q_1)v_b + (q_1+q_2)v_c \\ v_{c_2} = f_3(v_a, v_b, v_c) = (q_1+q_2)v_a - q_2 v_b + (1-q_1)v_c \end{cases}$$

$$\begin{cases} v_{a_3} = f_4(v_a, v_b, v_c) = (1-q_1)v_a - q_2 v_b + (q_1+q_2)v_c \\ v_{b_3} = f_5(v_a, v_b, v_c) = (q_1+q_2)v_a + (1-q_1)v_b - q_2 v_c \\ v_{c_3} = f_6(v_a, v_b, v_c) = -q_2 v_a + (q_1+q_2)v_b + (1-q_1)v_c \end{cases} \tag{27}$$

where,

$$\begin{cases} q_1 = N_{p1}/N_p = 0.258;\ q_2 = N_s/N_p = 0.137 \\ N_p = 2N_{p1} + N_{p2} \end{cases} \tag{28}$$

$N_{p1}$, $N_P$, $N_{p2}$, and $N_s$ are the corresponding winding turn, as shown in Fig. 9.

According to Kirchhoff's current law and principle of magnetic potential balance, the relationship among the power side currents and the three sets of currents fed to diode bridges can be obtained as

$$\begin{cases} i_A = i_{a1} + (1-q_1)\cdot(i_{a2}+i_{a3}) - q_2\cdot(i_{b2}+i_{c3}) \\ \quad +(q_1+q_2)\cdot(i_{b3}+i_{c2}) \\ i_B = i_{b1} + (1-q_1)\cdot(i_{b2}+i_{b3}) - q_2\cdot(i_{c2}+i_{a3}) \\ \quad +(q_1+q_2)\cdot(i_{c3}+i_{a2}) \\ i_C = i_{c1} + (1-q_1)\cdot(i_{c2}+i_{c3}) - q_2\cdot(i_{a2}+i_{b3}) \\ \quad +(q_1+q_2)\cdot(i_{a3}+i_{b2}) \end{cases} \tag{29}$$

Based on Fig. 10, the switching functions of diode bridges are plotted in Fig. 11. For each diode in DB-1, the conducting period is $4\pi/9$. For each diode in DB-2 and DB-3, the conducting period is $\pi/9$.

The corresponding switching functions of DB-1, DB-2, and DB-3 can be derived in (30), as shown at the bottom of the next page. Thus, the relationship between the dc-link voltage and the three sets of input voltages can be written as shown in the following (31).

$$u_{dc} = (s_a v_a + s_b v_b + s_c v_c) + \left(s_{a_2} v_{a_2} + s_{b_2} v_{b_2} + s_{c_2} v_{c_2}\right) + \left(s_{a_3} v_{a_3} + s_{b_3} v_{b_3} + s_{c_3} v_{c_3}\right) \tag{31}$$

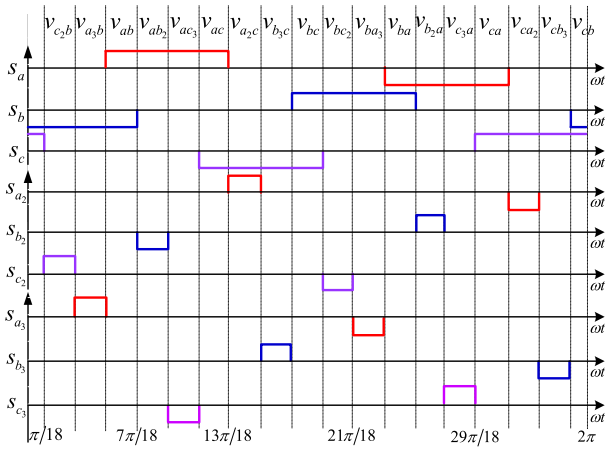


**FIGURE 11.** The switching functions of three groups diode bridges.

Then, $u_{\mathrm{dc}}$ can be transformed into the DP domain as below

$$\begin{aligned}&\langle u_{\mathrm{dc}}\rangle_k\\&=\left\{\langle s_a v_a\rangle_k+\langle s_b v_b\rangle_k+\langle s_c v_c\rangle_k\right\}\\&\quad+\left\{\left\langle s_{a_2} v_{a_2}\right\rangle_k+\left\langle s_{b_2} v_{b_2}\right\rangle_k+\left\langle s_{c_2} v_{c_2}\right\rangle_k\right\}\\&\quad+\left\{\left\langle s_{a_3} v_{a_3}\right\rangle_k+\left\langle s_{b_3} v_{b_3}\right\rangle_k+\left\langle s_{c_3} v_{c_3}\right\rangle_k\right\},\quad k=0,\pm2,\ldots\end{aligned}\tag{32}$$

Based on (27) and Euler formulate, the voltages fed to diode bridges in the DP domain can be derived. Similarly, the DPs of switching functions of three three-phase diode bridges can be obtained from (30).

For the asymmetrical 18-pulse AT-RU, $u_{\mathrm{dc}}$ mainly contains the dc component and 18th component under the balanced condition. The disturbance caused by unbalanced fault will appear in the form of harmonics, which are integer multiple of the 2nd harmonic component. The dominant $k$th($k=0,\pm2,\pm4,\pm18$) harmonics are retained to achieve fast and accurate simulation, while the other insignificant terms are neglected.

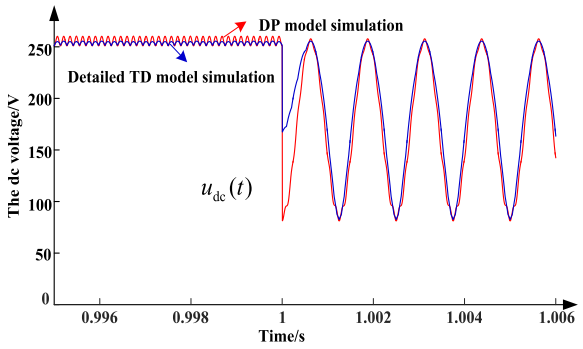


**FIGURE 12.** The dc side voltage of asymmetrical 18-pulse AT-RU.

The relationships among dc current and input currents of three three-phase diode bridges in DP domain are gained as

$$\begin{cases}\langle i_{a1}\rangle_k=\langle s_a i_{\mathrm{dc}}\rangle_k\\ \langle i_{b1}\rangle_k=\langle s_b i_{\mathrm{dc}}\rangle_k\\ \langle i_{c1}\rangle_k=\langle s_c i_{\mathrm{dc}}\rangle_k\end{cases}\quad\begin{cases}\langle i_{a2}\rangle_k=\langle s_{a2} i_{\mathrm{dc}}\rangle_k\\ \langle i_{b2}\rangle_k=\langle s_{b2} i_{\mathrm{dc}}\rangle_k\\ \langle i_{c2}\rangle_k=\langle s_{c2} i_{\mathrm{dc}}\rangle_k\end{cases}\quad\begin{cases}\langle i_{a3}\rangle_k=\langle s_{a3} i_{\mathrm{dc}}\rangle_k\\ \langle i_{b3}\rangle_k=\langle s_{b3} i_{\mathrm{dc}}\rangle_k\\ \langle i_{c3}\rangle_k=\langle s_{c3} i_{\mathrm{dc}}\rangle_k\end{cases}\tag{33}$$

The DPs of $i_{\mathrm{dc}}$ is available after getting $<u_{\mathrm{dc}}>_k$, the DPs of currents can be derived from (33), then the input currents in the power source side can be achieved from (29).

Assuming the RMS value of voltage source is 105V; the frequency is 400Hz; the dc side resistor load is $R=6\Omega$; the core type of AT is SR20kW; $N_{\mathrm{p1}}=67$; $N_{\mathrm{p2}}=125$; $N_{\mathrm{s}}=35$; $v_{\mathrm{A}}$ becomes zero at time $t=1.0$s. The AT in the detailed TD model is represented with fifteen dimensions mutual inductance matrix.

The dc side voltage $u_{\mathrm{dc}}(t)$ and ac side current $i_{\mathrm{A}}(t)$ obtained from the detailed TD model and the DP model are compared in Fig. 12 and Fig. 13, respectively.

$$\begin{aligned}s_a&=\sum_{n=1}^{\infty}\frac{\cos(5n\pi/18)}{n\pi}\left[-1-\cos(2n\pi)+2\cos(n\pi)\right]\cos(n\omega t+\frac{\pi}{2}),\quad n=1,3,5,7,\ldots\\ s_{a_2}&=\begin{cases}2\sqrt{2}\sum_{n=1}^{\infty}\frac{\sqrt{1-\cos(-n\pi/9)}}{n\pi}\cos\left[n\omega t-\frac{\pi}{2}-\arctan\frac{\sin(5n\pi/18)-\sin(3n\pi/18)}{\cos(3n\pi/18)-\cos(5n\pi/18)}\right], & n=1,3,11,13,\ldots\\ 2\sqrt{2}\sum_{n=1}^{\infty}\frac{\sqrt{1-\cos(-n\pi/9)}}{n\pi}\cos\left[n\omega t+\frac{\pi}{2}-\arctan\frac{\sin(5n\pi/18)-\sin(3n\pi/18)}{\cos(3n\pi/18)-\cos(5n\pi/18)}\right], & n=5,7,9,15,17,\ldots\end{cases}\\ s_{a_3}&=\begin{cases}2\sqrt{2}\sum_{n=1}^{\infty}\frac{\sqrt{1-\cos(-n\pi/9)}}{n\pi}\cos\left[n(\omega t+\frac{10}{18}\pi)-\frac{\pi}{2}-\arctan\frac{\sin(5n\pi/18)-\sin(3n\pi/18)}{\cos(3n\pi/18)-\cos(5n\pi/18)}\right], & n=1,3,11,13,\ldots\\ 2\sqrt{2}\sum_{n=1}^{\infty}\frac{\sqrt{1-\cos(-n\pi/9)}}{n\pi}\cos\left[n(\omega t+\frac{10}{18}\pi)+\frac{\pi}{2}-\arctan\frac{\sin(5n\pi/18)-\sin(3n\pi/18)}{\cos(3n\pi/18)-\cos(5n\pi/18)}\right], & n=5,7,9,15,17,\ldots\end{cases}\end{aligned}\tag{30}$$

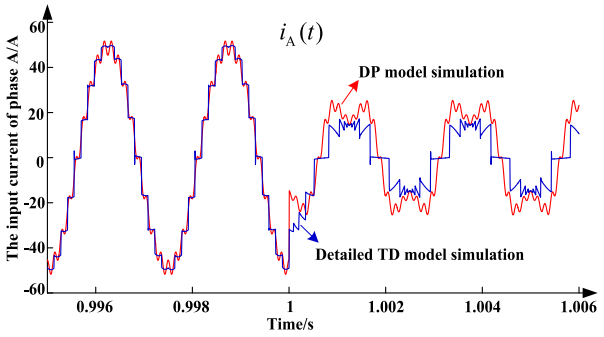


**FIGURE 13.** The ac side current of asymmetrical 18-pulse AT-RU.

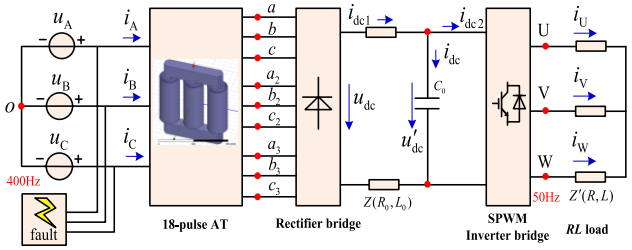


**FIGURE 14.** The circuit of VSI fed by asymmetrical 18-pulse AT-RU.

It can be known that the DP model can efficiently reflect the dynamic characteristic of asymmetrical 18-pulse AT-RU, under both balanced and unbalanced conditions.

## V. DP MODELLING FOR VSI FED BY 18-PULSE AT-RU

To verify the interfacing of the DP model of multipulse RU within extended EPS models, a voltage source inverter (VSI) fed by the asymmetrical 18-pulse AT-RU is studied. The circuit topology is shown in Fig. 14.

Fig. 15 illustrates the principle of the two-level Sinusoidal Pulse Width Modulation (SPWM) method.

By comparing the reference signal $U_r \sin(\omega_r t + \varphi)$ to the triangular carrier signal $u_c(t)$ with much higher frequency, the switching functions of inverter bridges in a period of the triangular carrier signal can be derived. Only $s_U(t)$ is given as

$$s_U(t) = \begin{cases} -1/2 & -\pi \le \omega_c t \le \theta_1 \\ 1/2 & \theta_1 \le \omega_c t \le \theta_2 \\ -1/2 & \theta_2 \le \omega_c t \le \pi \end{cases} \tag{34}$$

where $\theta_1$ can be derived by properties of similar triangular $\Delta$ ABC and $\Delta$ ADE, $\theta_2$ can be gained with the same way.

$$\begin{cases} \theta_1 = -\pi/2 - \pi/2 \cdot m \cdot \sin(\omega_r t + \varphi) \\ \theta_2 = \pi/2 + \pi/2 \cdot m \cdot \sin(\omega_r t + \varphi) \end{cases} \tag{35}$$

where $m$ is the modulation index.

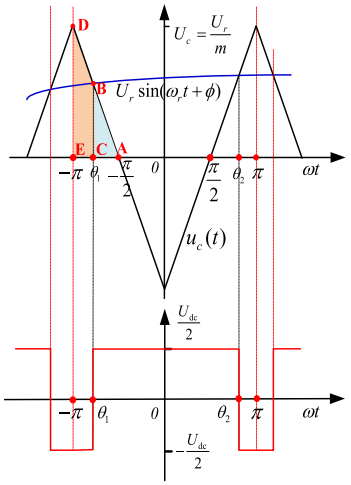


**FIGURE 15.** The principle of SPWM control strategy.

The Fourier series expansion of (34) is shown in (36), as shown at the bottom of this page.

Where the Bessel Function can be represented by

$$\begin{cases} J_p(x) = \sum_{m=0}^{\infty} (-1)^m / (m!\Gamma(p+m+1)) \cdot (x/2)^{2m+p} \\ \Gamma(p+m+1) = (p+m)! \end{cases} \tag{37}$$

The DP modelling of the rectifier part is detailed in Section IV. Thus, this section is mainly illustrating the DP modelling of the inverter part.

According to Fig. 14, the state-space equation at the inverter side can be written as (38).

$$\begin{aligned} \mathrm{d}i_U/\mathrm{d}t &= 1/L(u'_{dc} s_U - R i_U) \\ \mathrm{d}i_V/\mathrm{d}t &= 1/L(u'_{dc} s_V - R i_V) \\ \mathrm{d}i_W/\mathrm{d}t &= 1/L(u'_{dc} s_W - R i_W) \\ du'_{dc}/\mathrm{d}t &= 1/C\,(i_{dc1} - s_U i_U - s_V i_V - s_W i_W) \\ \mathrm{d}i_{dc1}/\mathrm{d}t &= -1/2L_0\left(u'_{dc} - u_{dc}\right) - R_0/L_0 i_{dc1} \end{aligned} \tag{38}$$

where $u_{dc}$ is the input of this state-space equation, and it is directly derived from (31).

In Fig. 14, supposing the frequency of power source $u_A$ ($u_B$, $u_C$) is 400Hz, the frequency of output terminal current $i_U$ ($i_V$, $i_W$) is 50Hz. It is knows that $u_{dc}(t)$ mainly contains dc component and 18th (7200Hz) harmonic component under balanced condition, and the 2nd harmonic (800Hz) will appear under unbalanced condition. To the inverter, the impact of high frequency 18th harmonic voltage in $u_{dc}(t)$ can be neglected. Here, the 2nd harmonic (800Hz) of $u_{dc}$ is

$$\begin{cases} s_{U,1} = 1/2 \cdot m \cdot \sin(\omega_r t + \phi) \\ s_{U,n,l} = \dfrac{1}{2} \cdot \sum\limits_{n=1}^{\infty} \left(\dfrac{4}{n\pi}\right) \left( \begin{array}{l} 2 \sum\limits_{l=1}^{\infty} J_{2l-1}\left(\frac{mn\pi}{2}\right) \sin\left[(2l-1)(\omega_r t + \phi)\right] \cos\frac{n\pi}{2} + \\ \left[ J_0\left(\frac{mn\pi}{2}\right) + 2 \sum\limits_{l=1}^{\infty} J_{2l}\left(\frac{mn\pi}{2}\right) \cos(2l)(\omega_r t + \phi) \right] \sin\frac{n\pi}{2} \end{array} \right) \cos(n\omega_c t) \end{cases} \tag{36}$$

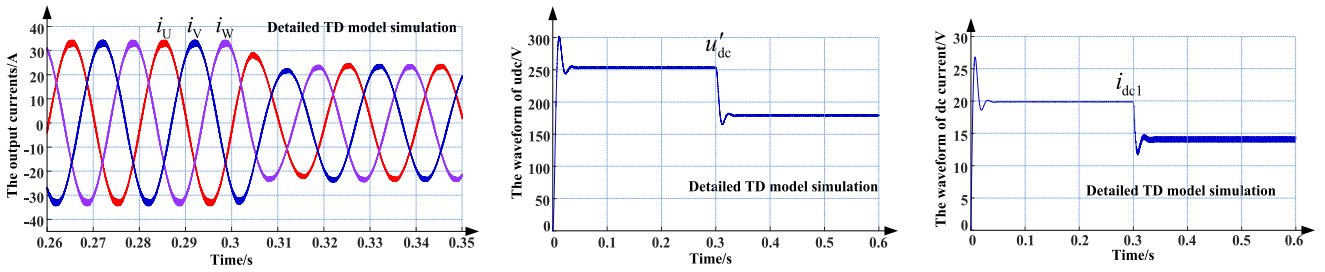


**FIGURE 16.** The simulation results obtained by the detailed TD model.

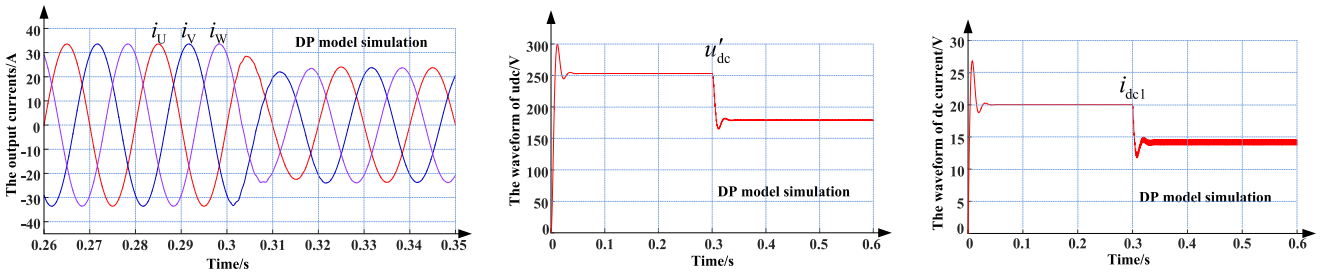


**FIGURE 17.** The simulation results obtained by the DP model.

renamed as 16th harmonic since the frequency of reference signal $U_r \sin(\omega_r t + \Phi)$ in Fig. 15 is 50Hz. Therefore, the DPs of $u_{dc}(t)$ are $< u_{dc} >_0$, $< u_{dc} >_{16}$ and $< u_{dc} >_{-16}$; the DPs of $u'_{dc}(t)$ are $<u'_{dc}>_0$, $<u'_{dc}>_{16}$, and $<u'_{dc}>_{-16}$; the DPs of $i_{dc1}(t)$ are $< i_{dc1} >_0$, $< i_{dc1} >_{16}$, and $< i_{dc1} >_{-16}$. High order harmonics will be eliminated by inductive loads, thus, the considered DPs of $s_U(t)$, $s_V(t)$, and $s_W(t)$ are $< s_U >_1$, $< s_U >_{-1}$, $< s_V >_1$, $< s_V >_{-1}$, $< s_W >_1$, and $< s_W >_{-1}$. The 16th component of $u'_{dc}(t)$ and the fundamental component of switching function are retained, since $i_U(t)$ is based on $u'_{dc}(t)$ and $s_U(t)$, the DPs of $i_U(t)$ are $< i_U >_1$, $< i_U >_{-1}$, $< i_U >_{15}$, $< i_U >_{-15}$, $< i_U >_{17}$, and $< i_U >_{-17}$.

Based on (4), (5), and (6), the state-space equation in the DP domain can be gained by replacing the time-domain variables in (38) with their DPs [19], [20]. The real and imaginary parts of DPs are furtherly separated to improve the calculation speed. Since the whole state-space equation in the DP domain is too large to show here, only the DP domain equations of $di_U/dt$ are presented in (39).

$$
\begin{aligned}
\frac{\mathrm{d}\langle i_U\rangle_1^R}{\mathrm{d}t} &= -\frac{R}{L}\langle i_U\rangle_1^R + \omega\langle i_U\rangle_1^I + \frac{1}{L}\langle u'_{dc}\rangle_0\langle s_U\rangle_1^R \\
\frac{\mathrm{d}\langle i_U\rangle_1^I}{\mathrm{d}t} &= -\omega\langle i_U\rangle_1^R - \frac{R}{L}\langle i_U\rangle_1^I + \frac{1}{L}\langle u'_{dc}\rangle_0\langle s_U\rangle_1^I \\
\frac{\mathrm{d}\langle i_U\rangle_{15}^R}{\mathrm{d}t} &= -\frac{R}{L}\langle i_U\rangle_{15}^R + 15\cdot\omega\langle i_U\rangle_{15}^I \\
&\quad + \frac{1}{L}\left[\langle u'_{dc}\rangle_{16}^R\langle s_U\rangle_1^R + \langle u'_{dc}\rangle_{16}^I\langle s_U\rangle_1^I\right] \\
\frac{\mathrm{d}\langle i_U\rangle_{15}^I}{\mathrm{d}t} &= -15\cdot\omega\langle i_U\rangle_{15}^R \\
&\quad - \frac{R}{L}\langle i_U\rangle_{15}^I - \frac{1}{L}\left[\langle u'_{dc}\rangle_{16}^R\langle s_U\rangle_1^I - \langle u'_{dc}\rangle_{16}^I\langle s_U\rangle_1^R\right] \\
\frac{\mathrm{d}\langle i_U\rangle_{17}^R}{\mathrm{d}t} &= -\frac{R}{L}\langle i_U\rangle_{17}^R + 17\cdot\omega\langle i_U\rangle_{17}^I \\
&\quad + \frac{1}{L}\left[\langle u'_{dc}\rangle_{16}^R\langle s_U\rangle_1^R - \langle u'_{dc}\rangle_{16}^I\langle s_U\rangle_1^I\right] \\
\frac{\mathrm{d}\langle i_U\rangle_{17}^I}{\mathrm{d}t} &= -17\cdot\omega\langle i_U\rangle_{15}^R - \frac{R}{L}\langle i_U\rangle_{17}^I \\
&\quad + \frac{1}{L}\left[\langle u'_{dc}\rangle_{16}^R\langle s_U\rangle_1^I + \langle u'_{dc}\rangle_{16}^I\langle s_U\rangle_1^R\right]
\end{aligned}
\tag{39}
$$

As illustrated in Fig. 3, the negative DPs do not contain any additional information of the time-domain signal. Here, only positive orders of DPs are applied.

Assuming the parameters of asymmetrical 18-pulse AT-RU are the same as that given in section IV, $u_A$ becomes zero at time $t = 0.3$s. The smoothing reactor $Z$ is with $R_0 = 0.02\Omega$ and $L_0 = 20$mH; $C_0 = 300\mu$F; the $RL$ load consists of $R = 3\Omega$ and $L = 1$mH. To the carrier-based two-level SPWM method, the frequency of carrier signal is $f_c = 10$kHz; the frequency of reference signal is $f_r = 50$Hz; the minimum and maximum values of the carrier signal are $-1$ and 1; the modulation index is 0.8.

By using the detailed TD simulation model and the DP simulation model, the waveforms of state-space variables $i_U$, $i_V$, $i_W$, $u'_{dc}$, and $i_{dc1}$ are plotted in Fig. 16 and Fig. 17, respectively. Meanwhile, the power source side current $i_A$ and the dc-link voltage $u_{dc}$ in the rectifier side are drawn in Fig. 18.

All these results reveal that the DP model can accurately reflect the dynamic characteristics of VSI fed by the 18-pulse asymmetrical AT-RU, under both balanced and unbalanced conditions.

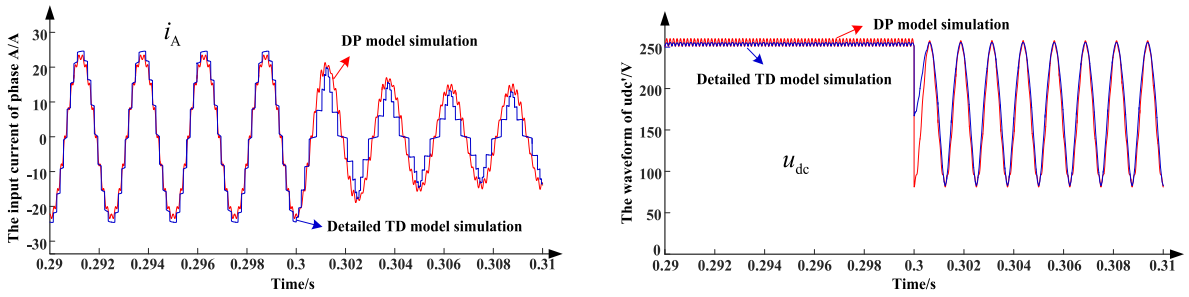


**FIGURE 18.** The waveforms of input current $i_A$ and dc side voltage $u_{dc}$ obtained by the two methods.

**TABLE 1.** The computation efficiency comparision.

| The type of converter syetem | 12-Pulse PSR-RU | 18-Pulse AT-RU | VSI fed by 18-pulse AT-RU |
|---|---|---|---|
| Simulation Stop time(s) | 2.0 | 2.0 | 0.6 |
| Computation time(s): $t_{TD}$ | 32.1 | 188.6 | 550.3 |
| Computation time(s): $t_{DP}$ | 1.9 | 16.7 | 21.9 |
| Acceleration factor: $t_{TD}/t_{DP}$ | 16.9 | 11.3 | 25.1 |
| THD($i_A$)% of DP model | 10.22 | 8.28 | 7.34 |
| THD($i_A$)% of TD model | 10.05 | 8.01 | 7.01 |
| Error of THD($i_A$)% | 0.17 | 0.27 | 0.33 |
| $\rho(i_A)$ of TD and DP model | 0.9536 | 0.9565 | 0.9727 |
| $\rho(u_{dc})$ of TD and DP model | 0.9981 | 0.9918 | 0.9920 |

## VI. COMPUTATION EFFICIENCY OF DP MODELLING

The DP models are coded with m-file in MATLAB, and the detailed TD models are built with MATLAB/Simulink. The computation time is recorded by the software automatically.

In TABLE 1, $t_{TD}$ and $t_{DP}$ are the computation time of the two models. The DP model for symmetrical 12-pulse PSR-RU achieves 16.9 times faster computation time than the detailed TD model, and this acceleration factor becomes 11.3 times and 25.1 times for the asymmetrical 18-pulse AT-RU and the VSI fed by asymmetrical 18-pulse AT-RU. The total harmonic distortion (THD) of $i_A$ under the balanced condition is also analyzed, and the maximum error between the DP simulation and the detailed TD simulation is about 0.33%. $\rho(i_A)$ and $\rho(u_{dc})$ are Pearson's correlation coefficient of waveforms $i_A$ and $u_{dc}$ obtained by DP and TD models. All of them are close to 1, showing that the DP models achieve a good calculation accuracy.

## VII. CONCLUSION

The accurate and fast simulation models of the various multipulse rectifier units and the VSI fed by asymmetrical 18-pulse AT-RU are proposed in this paper. The diode bridges of the 12-pulse PSR-RU can be simplified to two three-phase diode bridges due to the symmetrical properties, and derivation of the DP model is based on the relations between ac and dc terminals. This approach is useful for the DP modelling of symmetrical multipulse rectifiers. The DP modelling of asymmetrical 18-pulse AT-RU is mainly based on the switching functions expressed in the DP domain. This way applies to all kinds of multipulse rectifiers. To the VSI fed by asymmetrical 18-pulse AT-RU, the dynamic performance is revealed by solving the state-space equations in the DP domain. This method may result in huge size equations for an extensive power conversion system.

The efficiency of proposed three DP models are verified by the detailed TD models, respectively. The proposed DP models achieve at least 11.3 times faster computation time than the detailed TD model. The maximum error of ac side current harmonic distortion between the DP model and the detailed TD model is 0.33%.

The proposed DP models cover the various multipulse rectifier units, and can be used as library elements interfacing within extended EPS models such as the VSI given in this paper. Predictably, the efficiency of the DP model will become increasingly apparent for a much more complicated power electronics dominated power system.

## REFERENCES

[1] D. Shu, X. Xie, Z. Yan, V. Dinavahi, and K. Strunz, "A multi-domain co-simulation method for comprehensive shifted-frequency phasor DC-grid models and EMT AC-grid models," *IEEE Trans. Power Electron.*, vol. 34, no. 11, pp. 10557–10574, Nov. 2019.

[2] L. Wang, X. Deng, P. Han, X. Qi, X. Wu, M. Li, and H. Xu, "Electromagnetic transient modeling and simulation of power converters based on a piecewise generalized state space averaging method," *IEEE Access*, vol. 7, pp. 12241–12251, 2019.

[3] G. Bilal, P. Gomez, R. Salcedo, and J. M. Villanueva-Ramirez, "Electromagnetic transient studies of large distribution systems using frequency domain modeling methods and network reduction techniques," *Int. J. Electr. Power Energy Syst.*, vol. 110, pp. 11–20, Sep. 2019.

[4] H. Ye and K. Strunz, "Multi-scale and frequency-dependent modeling of electric power transmission lines," *IEEE Trans. Power Del.*, vol. 33, no. 1, pp. 32–41, Feb. 2018.

[5] J. B. Kwon, X. Wang, F. Blaabjerg, and C. L. Bak, "Frequency domain modelling and simulation of DC power electronic systems," *IEEE Trans. Power Electron.*, vol. 32, no. 2, pp. 1044–1055, Feb. 2017.

[6] Y. Huang, S. Ebrahimi, N. Amiri, Z. Shan, and J. Jatskevich, "Parametric dynamic phasor modeling of thyristor-controlled rectifier systems including harmonics for various operating modes," *IEEE Trans. Energy Convers.*, vol. 32, no. 4, pp. 1626–1629, Dec. 2017.

[7] Y. Zhang, Z. Chen, B. Li, and Y. He, "Application of low harmonic 18-pulse rectifier power supply for radar power system," *IEEE Trans. Ind. Electron.*, vol. 66, no. 2, pp. 1080–1088, Feb. 2019.

[8] B. Singh, S. Gairola, B. N. Singh, A. Chandra, and K. Al-Haddad, "Multipulse AC–DC converters for improving power quality: A review," *IEEE Trans. Power Electron.*, vol. 23, no. 1, pp. 260–281, Jan. 2008.

[9] F. Meng, L. Gao, S. Yang, and W. Yang, "Effect of phase-shift angle on a delta-connected autotransformer applied to a 12-pulse rectifier," *IEEE Trans. Ind. Electron.*, vol. 62, no. 8, pp. 4678–4690, Aug. 2015.

[10] F. Meng, W. Yang, Y. Zhu, L. Gao, and S. Yang, "Load adaptability of active harmonic reduction for 12-pulse diode bridge rectifier with active interphase reactor," *IEEE Trans. Power Electron.*, vol. 30, no. 12, pp. 7170–7180, Dec. 2015.
[11] D. Yuan, S. Wang, H. Li, S. Wang, and S. Wang, "Simulation analysis and development of industrial design software of phase-shifting reactor used in the 6-phase rectifier system," in *Proc. 20th Int. Conf. Electr. Mach. Syst. (ICEMS)*, Sydney, NSW, Australia, Aug. 2017, pp. 1–5.
[12] T. Yang, S. Bozhko, and G. Asher, "Functional modeling of symmetrical multipulse autotransformer rectifier units for aerospace applications," *IEEE Trans. Power Electron.*, vol. 30, no. 9, pp. 4704–4713, Sep. 2015.
[13] T. Wu, S. V. Bozhko, G. M. Asher, and D. W. P. Thomas, "A fast dynamic phasor model of autotransformer rectifier unit for more electric aircraft," in *Proc. 35th Annu. Conf. IEEE Ind. Electron.*, Porto, Portugal, Nov. 2009, pp. 2531–2536.
[14] S. R. Sanders, J. M. Noworolski, X. Z. Liu, and G. C. Verghese, "Generalized averaging method for power conversion circuits," *IEEE Trans. Power Electron.*, vol. 6, no. 2, pp. 251–259, Apr. 1991.
[15] J. R. C. Orillaza and A. R. Wood, "Harmonic state-space model of a controlled TCR," *IEEE Trans. Power Del.*, vol. 28, no. 1, pp. 197–205, Jan. 2013.
[16] C. Liu, A. Bose, and P. Tian, "Modeling and analysis of HVDC converter by three-phase dynamic phasor," *IEEE Trans. Power Del.*, vol. 29, no. 1, pp. 3–12, Feb. 2014.
[17] T. Yang, S. Bozhko, J.-M. Le-Peuvedic, G. Asher, and C. I. Hill, "Dynamic phasor modeling of multi-generator variable frequency electrical power systems," *IEEE Trans. Power Syst.*, vol. 31, no. 1, pp. 563–571, Jan. 2016.
[18] T. Yang, S. Bozhko, and G. Asher, "Fast functional modelling of diode-bridge rectifier using dynamic phasors," *IET Power Electron.*, vol. 8, no. 6, pp. 947–956, Jun. 2015.
[19] J. Kwon, X. Wang, F. Blaabjerg, C. L. Bak, A. R. Wood, and N. R. Watson, "Harmonic instability analysis of a single-phase grid-connected converter using a harmonic state-space modelling method," *IEEE Trans. Ind. Appl.*, vol. 52, no. 5, pp. 4188–4200, Sep. 2016.
[20] J. B. Kwon, X. F. Wang, F. Blaabjerg, C. L. Bak, V. S. Sularea, and C. Busca, "Harmonic interaction analysis in a grid-connected converter using harmonic state-space (HSS) modelling," *IEEE Trans. Power Electron.*, vol. 32, no. 9, pp. 6823–6835, Sep. 2017.
[21] J. Lyu, X. Zhang, X. Cai, and M. Molinas, "Harmonic state-space based small-signal impedance modeling of a modular multilevel converter with consideration of internal harmonic dynamics," *IEEE Trans. Power Electron.*, vol. 34, no. 3, pp. 2134–2148, Mar. 2019.
[22] J. B. Kwon, X. Wang, C. L. Bak, and F. Blaabjerg, "Modeling and simulation of DC power electronics systems using harmonic state space (HSS) method," in *Proc. IEEE 16th Workshop Control Modeling Power Electron. (COMPEL)*, Vancouver, BC, Canada, Jul. 2015, pp. 1–8.
[23] M. Esparza, J. Segundo-Ramirez, J. B. Kwon, X. Wang, and F. Blaabjerg, "Modeling of VSC-based power systems in the extended harmonic domain," *IEEE Trans. Power Electron.*, vol. 32, no. 8, pp. 5907–5916, Aug. 2017.

**DONGSHENG YUAN** (Student Member, IEEE) received the B.S. and M.S. degrees in electrical engineering from Lanzhou Jiaotong University, Lanzhou, China, in 2010 and 2014, respectively. He is currently pursuing the Ph.D. degree with the School of Electrical Engineering, Xi'an Jiaotong University, Xi'an, China. He was a Visiting Student with the Department of Electrical Engineering and Computer Science, The University of Tennessee at Knoxville, Knoxville, TN, USA, from 2017 to 2019. His current research interest includes elctromagnetic devices and fast functional modeling of power converter systems.

**SHUHONG WANG** (Senior Member, IEEE) received the B.S., M.S., and Ph.D. degrees in electrical engineering from Xi'an Jiaotong University, Xi'an, in 1990, 1993, and 2002, respectively. He was a Postdoctoral Fellow with the Department of Mechatronics, Gwangju Institute of Science and Technology, Gwangju, South Korea, from 2004 to 2005. He was a Research Fellow with the Faculty of Engineering, University of Technology at Sydney, Sydney, NSW, Australia, in 2005. His current research interests include the theory of circuit, electromagnetic field, and multiphysics field, numerical analysis methods, the design, simulation, and optimization of energy-efficient power conversion and transmission equipment and special electromagnetic devices, and modeling and simulation of the electromagnetic properties of advanced electrical materials.

**YILU LIU** (Fellow, IEEE) received the B.S. degree from Xi'an Jiaotong University, Xi'an, China, and the M.S. and Ph.D. degrees from The Ohio State University, Columbus, OH, USA, in 1986 and 1989, respectively. She is currently the Governor's Chair with The University of Tennessee at Knoxville, Knoxville, TN, USA, and the Oak Ridge National Laboratory (ORNL). She is also the Deputy Director of the DOE/NSF co-funded Engineering Research Center (CURENT). Prior to joining UTK/ORNL, she was a Professor at Virginia Tech. She led the effort to create the North American power grid frequency monitoring network at Virginia Tech, which is currently operated at UTK and ORNL as GridEye. Her current research interests include power system wide-area monitoring and control, large interconnection-level dynamic simulations, electromagnetic transient analysis, and power transformer modeling and diagnosis. She was elected as a member of the National Academy of Engineering, in 2016.